JAST, Vol. 3, No. 2, pp 77–85

JAST
Journal of Aerospace Science and Technology

Numerical Solution of Parabolized Stability Equations Using Super-Compact Scheme

V. Esfahanian[1], S. Ghader[2]

The super-compact finite difference method is used to develop a highly accurate finite difference PSE code to investigate the stability analysis of incompressible boundary layers over a flat plate. The PSE equations are derived in terms of primitive variables and are solved numerically using super compact method. In these formulations, both nonparallel as well as nonlinear effects are accounted for. The validity of the present numerical scheme is demonstrated using spatial simulations of two cases; two-dimensional (linear and nonlinear) Tollmien-Schlichting wave propagation and three-dimensional subharmonic instability breakdown. The PSE solutions have been compared with previous numerical investigations and experimental results and show good agreement.

INTRODUCTION

The objective of the present work is to develop an accurate and cost efficient way to investigate the stability and transition computation of incompressible boundary layers on a flat plate. There are several ways to predict transitions such as the linear stability theory, and direct Navier-Stokes solutions.

The hydrodynamic stability theory is useful in indicating the major dominant effects which hasten or delay transition in a relative sense. Some basic understanding of the transition problem in incompressible boundary layers can be reached using linear stability theory with the assumption of parallel flow. In addition, the transition location can be approximately predicted using an empirical correlation such as the e^N method. The usefulness of linear stability analysis is limited by inaccuracies due to the parallel flow approximation. Also, it is limited by the fact that latter stages of transition are nonlinear.

As a transition prediction tool, the direct numerical simulations (DNS) using full Navier-Stokes equations can accurately model the early stages of transition but require far too much computer power. Moreover, they have been obtained only for very simple geometries such as flat plate. Therefore, they are not appropriate for studying transition over complex geometries.

A new methodology for transition prediction which has been proposed by Herbert [1,2], Bertolotti [3] also Chang et al. [4] utilizes the Parabolized Stability Equations (PSE). Contrary to the linear stability theory, the PSE can be used to study nonparallel as well as nonlinear evolution of convective disturbances in growing boundary layers. In addition, the PSE does not need an empirical correlation to predict the transition location.

The PSE constitute nonlinear parabolized partial differential equations used to predict the laminar-turbulent transition. Similar to classical stability analysis, the PSE assume that transition process starts with the small disturbances amplifications. Since the PSE are nonlinear equations, they are valid for the finite-amplitude disturbances. But they are limited to flows with slowly varying properties in the streamwise direction.

The PSE are an initial-boundary value problem and they can be solved using a marching procedure. As a result, the computational effort and required storage can be reduced using the PSE. Therefore, these equations are appropriate for a rapid and accurate prediction of laminar-turbulent transition of incompressible boundary layers.

In this context, the computation of the stability and onset of transition location of incompressible flow over a flat plate based on linear and nonlinear PSE using super compact scheme and primitive vari-

1. *Associate Professor, Dept. of Mech. Eng., Tehran Univ., Tehran, Iran, Email: evahid@ut.ac.ir.*
2. *Assistant Professor, Institute of Geophysics, Tehran Univ., Tehran, Iran, Email: sghader@ut.ac.ir.*

ables is performed. Two cases are computed by the PSE theory: two-dimensional (linear and nonlinear) Tollmien-Schlichting (TS) wave propagation and three-dimensional subharmonic breakdown. The present computations are compared with available numerical, DNS and experimental results.

PROBLEM FORMULATION

In this study, the stability of incompressible flow over a flat plate in Cartesian coordinate system is formulated. The Cartesian coordinates are denoted by x, y, and z, where x is the streamwise distance from the leading edge, and y and z are the plate normal and the spanwise coordinates, respectively. All quantities are nondimensionalized with the free stream velocity U_∞ and the fixed length $\delta_\circ = \delta(x_\circ) = \sqrt{\nu x_\circ / U_\infty}$, where $x_\circ$ is a fixed starting dimensional distance from the leading edge and ν is kinematic viscosity. The resulting nondimensional parameter is the reference Reynolds number $R_\circ = U_\infty \delta_\circ / \nu$ at $x = x_\circ$ (Bertolotti et al., [5]). Then, the three dimensional incompressible Navier-Stokes equations in the nondimensional form are as follows:

$$\nabla \cdot V = 0, \tag{1}$$

$$\frac{\partial V}{\partial t} + (V \cdot \nabla)V = -\nabla p + \frac{1}{R_\circ}\nabla^2 V, \tag{2}$$

where $V = (u, v, w)$ is the velocity vector and p is the pressure.

To obtain the disturbance equations, one can split the dependent quantities vector $\phi = (u, v, w, p)^T$ into a steady two-dimensional mean value (basic flow) $\Phi_b = (U_b, V_b, 0, P_b)^T$ and an unsteady three-dimensional perturbation quantity $\phi' = (u', v', w', p')^T$ i.e.,

$$\phi(x, y, z, t) = \Phi_b(x, y) + \phi'(x, y, z, t). \tag{3}$$

By substituting the vector ϕ into the Navier-Stokes equations (1) and (2), and subtracting the terms satisfied by the basic flow, one will obtain the governing equations for the disturbances ϕ', which will not be presented here (for example see Reference [18]).

Basic Flow

For flow over the flat plate the basic flow can be obtained by solving the self-similar boundary layer equations (the Blasius equation):

$$f''' + \frac{1}{2} f f'' = 0, \tag{4}$$

with boundary conditions:

$f(0) = f'(0) = 0, \quad f'(\infty) = 1.$

where $f(\eta)$ is the Blasius function defined as:

$$\Psi_b = \sqrt{\nu U_\infty x} f(\eta), \quad \eta = y\sqrt{\frac{U_\infty}{\nu x}},$$

and Ψ_b is the stream function of the basic flow.

Linear PSE

One way to derive the PSE, as suggested by Herbert and Bertolotti [6] is to decompose disturbances into a rapidly varying wave-like part and a slowly growing shape function. The ellipticity is retained for the wave part while the parabolization is applied to the shape function. For linear PSE, one can assume that the disturbance vector ϕ' for an instability wave with a frequency ω and a spanwise wave number β can be expressed as:

$$\phi'(x, y, z, t) = \hat{\phi}(x, y)\chi(x, z, t), \tag{5}$$

where the shape function vector $\hat{\phi}$ and χ are:

$$\hat{\phi} = (\hat{u}, \hat{v}, \hat{w}, \hat{p})^T,$$

$$\chi = \exp\left(\int_{x_\circ}^{x} \alpha(s)ds + i\beta z - i\omega t\right).$$

The shape function $\hat{\phi}$ is a function of both x and y due to the growth of the boundary layer and the streamwise wave number α is a function of x to permit the growth of the boundary layer.

The linearized PSE are obtained by substituting the disturbance vector ϕ' into the linear disturbance equations. With the following essential property; characteristics of the flow such as velocity profiles, wavelengths and growth rates change slowly in the streamwise direction. Therefore, the shape function $\hat{\phi}$ along the streamwise direction changes such that the second derivatives of $\hat{\phi}$ ($\hat{\phi}_{xx}$) are negligible. Then, the linearized equations that describe the evolution of the shape function $\hat{\phi}$ will be obtained as fallows:

$$\alpha\hat{u} + \hat{u}_x + \hat{v}_y + i\beta\hat{w} = 0,$$

$$\mathcal{L}\hat{u} + \hat{u}U_{bx} + \hat{v}U_{by} + \alpha\hat{p} + \hat{p}_x = 0,$$

$$\mathcal{L}\hat{v} + \hat{v}V_{by} + \hat{p}_y = 0,$$

$$\mathcal{L}\hat{w} + i\beta\hat{p} = 0,$$

where

$$\mathcal{L} \equiv -i\omega + \alpha U_b + U_b\frac{\partial}{\partial x} + V_b\frac{\partial}{\partial y} - (\alpha^2 + \frac{\partial^2}{\partial y^2} - \beta^2)/R_\circ.$$

These equations can be written as a system of differential equations in terms of stability variables $\hat{q}$ as follows:

$$L(\alpha)[\hat{q}] + M(\alpha)[\frac{\partial \hat{q}}{\partial x}] = 0, \tag{6}$$

where $\hat{q} = (\hat{u}, \hat{v}, \hat{w}, \hat{p})^T$ and the operator matrices L

and M are defined in the following form:

$$L = \begin{pmatrix} \alpha & \frac{\partial}{\partial y} & i\beta & 0 \\ \tilde{\mathcal{L}} + \frac{\partial U_b}{\partial x} & \frac{\partial U_b}{\partial y} & 0 & \alpha \\ 0 & \tilde{\mathcal{L}} + \frac{\partial U_b}{\partial y} & 0 & \frac{\partial}{\partial y} \\ 0 & 0 & \tilde{\mathcal{L}} & i\beta \end{pmatrix},$$

$$M = \begin{pmatrix} 1 & 0 & 0 & 0 \\ U_b & 0 & 0 & 1 \\ 0 & U_b & 0 & 0 \\ 0 & 0 & U_b & 0 \end{pmatrix},$$

in which

$$\tilde{\mathcal{L}} \equiv -i\omega + \alpha U_b + V_b \frac{\partial}{\partial y} - (\alpha^2 + \frac{\partial^2}{\partial y^2} - \beta^2)/R_\circ.$$

Now, a scalar equation is needed to close the system. This equation must resolve the ambiguity created by the dependency of both $\hat{\phi}$ and α on x. This condition is called "auxiliary" condition, and in general can be expressed as follows:

$$\int_0^y \hat{q}^\dagger \cdot \frac{\partial \hat{q}}{\partial x} dy = 0, \tag{7}$$

where the components of vector $\hat{q}$ are $(\hat{u}, \hat{v}, \hat{w})$ ($\dagger$ denotes complex conjugate). The success of a marching solution would require a proper way of updating the wave number. Here, the wave number is updated as follows:

$$\alpha_{\text{new}} = \alpha_{\text{old}} - \frac{i \int \hat{u}^\dagger \frac{\partial \hat{u}}{\partial x} dy}{\int |\hat{u}|^2 dy}. \tag{8}$$

In the nonparallel boundary layers, the growth and phase variation of some physical quantity ψ depends on α and $\hat{\phi}$. Therefore, the physical growth rate $\bar{\gamma}$ and the physical wave number $\bar{\alpha}$ for any given flow variable ψ (such as $\hat{u}$,$\hat{v}$, etc.) are defined as:

$$\bar{\gamma}(x) = -\mathcal{I}[\alpha(x)] + \mathcal{R}\left[\frac{1}{\psi}\frac{\partial \psi}{\partial x}\right], \tag{9}$$

$$\bar{\alpha}(x) = \mathcal{R}[\alpha(x)] + \mathcal{I}\left[\frac{1}{\psi}\frac{\partial \psi}{\partial x}\right]. \tag{10}$$

According to these equations, the growth rate and the wave number depends upon the wall normal distance. Usually, these quantities are computed at the corresponding location where the fluctuation reaches its maximum value. For incompressible flow, the growth rate and the wave number are computed using the streamwise velocity shape function ($\psi = \hat{u}$).

The solution of linearized PSE equations (6) requires appropriate boundary conditions in the y-direction. At the wall, the components of perturbation velocity satisfy the no-slip condition:

$$\hat{u} = \hat{v} = \hat{w} = 0, \quad y = 0, \tag{11}$$

and the Dirichlet conditions are applied in the free-stream:

$$\hat{u} = \hat{v} = \hat{w} = 0, \quad y \to \infty. \tag{12}$$

For incompressible flows, some residual ellipticity exists, which can result in numerical instability in the marching procedure for small stepsizes. Therefore, the marching procedure will remain stable when the stepsize exceeds from the certain minimum value ($\Delta x > \Delta x_{\min}$).

Nonlinear PSE

In the linear PSE, the disturbance amplitude is assumed to be infinitesimally small so that the nonlinear interaction of these waves is negligible. For nonlinear waves, the total disturbance is assumed to be periodic in time and in the spanwise direction. For most problems, it is sufficient to choose a finite number of modes. In these cases, the total disturbance vector $\phi'(x, y, z, t)$ can be expressed as follows:

$$\phi' = \sum_{n=-N}^{N} \sum_{k=-K}^{K} \hat{\phi}_{nk}(x, y) \chi_{nk}(x, z, t), \tag{13}$$

where the shape function vector $\hat{\phi}_{nk}$ and χ_{nk} are:

$$\hat{\phi}_{nk} = (\hat{u}_{nk}, \hat{v}_{nk}, \hat{w}_{nk}, \hat{p}_{nk})^T,$$

$$\chi_{nk} = \exp\left[i\left(\int_{x_\circ}^{x} \alpha_{nk}(s) ds + k\beta z - n\omega t\right)\right].$$

The nonlinear PSE are obtained by substituting the disturbance vector ϕ' into the nonlinear disturbance equations and performing harmonic balance for both linear and nonlinear terms. Finally, the nonlinear PSE equations can be obtained for the shape function $\hat{\phi}_{nk}$ of a single Fourier mode (n, k), which can be written as a system of differential equations in terms of stability variables $\hat{q}_{nk}$ as follows:

$$L(\alpha_{nk})[\hat{q}_{nk}] + M(\alpha_{nk})\left[\frac{\partial \hat{q}_{nk}}{\partial x}\right] = H_{nk}, \tag{14}$$

where H_{nk} is nonlinear forcing function. The nonlinear PSE for a single Fourier mode is equivalent to the linear PSE with a frequency $n\omega$ and a spanwise wave number $k\beta$ with the additional forcing function H_{nk}.

The procedure for determination of wave number α_{nk} is similar to the linear PSE. For present computation, all modes are assumed to have the same phase

speed (phase-locked condition) i.e.,

$$\alpha_{nk} = \Big(n\mathcal{R}(\alpha_F), \mathcal{I}(\alpha_{nk})\Big), \tag{15}$$

where α_F is the fundamental TS wave, which is a function of x. The calculation of α_{nk} is similar to the linear case according to relation (8). For the detuned case the computation procedure is more complicated in the sense that mode bookkeeping becomes more cumbersome.

The solution procedure of the linear PSE can be applied to the nonlinear PSE, except for the modes with zero frequency ($n = 0$). These zero frequency modes are denoted as the mean flow distortion (MFD) ($k = 0$) or longitudinal vortex ($k \neq 0$). The boundary conditions (10) and (11) can be applied to the longitudinal vortex mode (zero frequency and non-zero spanwise wave number) without modification. For the MFD mode, the free stream boundary condition for normal velocity is replaced with Neumann condition to allow the mean flow to adjust itself for mass balance:

$$\hat{u}_{00} = \frac{\partial \hat{v}_{00}}{\partial y} = \hat{w}_{00} = 0, \quad y \to \infty. \tag{16}$$

This would allow the boundary layer to have the correct mass balance (or displacement thickness) due to the modification of mean flow ($U_b + \hat{u}_{00}$) caused by nonlinear mode interactions.

The new mode is generated into the field whenever the maximum magnitude of the corresponding nonlinear term is greater than a threshold (10^{-6}). Similarly, a mode is removed when the corresponding nonlinear term is less than the threshold and has a negative growth rate.

SUPER-COMPACT METHOD

The 'super-compact finite difference method' (SCFDM) is a highly accurate finite difference scheme of arbitrary order with minimal stencil size which has been introduced by Fu Dexun and Ma Yanwen [7]. The derivation and the application of the method in uniform grid have been presented by Ma Yanwen and Fu Dexun [8] and by Fu Dexun and Ma Yanwen [9]. In addition, some aspects of the scheme in nonuniform grid have been investigated by Ghader [10] and Esfahanian et al. [11]. Furthermore, Esfahanian et al. [12] have introduced the application of SCFDM for geophysical fluid dynamics problems.

This method has two general equations, namely the basic equation and the auxiliary equations. The basic equation is obtained by using Taylor series which relates a function f to its derivatives. In the basic equation there is a greater number of unknowns than equations, so auxiliary equations are needed to relate each derivative of f to the other derivatives. The basic equation, in a nonuniform grid, is:

$$(\alpha\delta_x^+ + \beta\delta_x^-)f_j = \frac{1}{1!}[\alpha + \beta\sigma_j]f_j^{<1>} + \frac{1}{2!}[\alpha - \beta\sigma_j^2]f_j^{<2>} + \ldots + \frac{1}{n!}[\alpha + (-1)^{n+1}\beta\sigma_j^n]f_j^{<n>}, \tag{17}$$

and the auxiliary equations are:

$$\sigma_{j+1}^l f_{j+1}^{<l>} - 2f_j^{<l>} + \frac{1}{\sigma_j^l} f_{j-1}^{<l>} = \frac{1}{1!}(1-\sigma_j)f_j^{<l+1>} + \frac{1}{2!}(1+\sigma_j^2)f_j^{<l+2>} + \ldots + \frac{1}{(n-l)!}(1+(-1)^{n-l}\sigma_j^{n-l})f_j^{<n>}, \tag{18}$$

where

$$\delta_x^+ f_j = f_{j+1} - f_j, \quad \delta_x^- f_j = f_j - f_{j-1}, \quad h_j = x_{j+1} - x_j,$$

$$\sigma_j = \frac{h_{j-1}}{h_j}, \quad f_j^{<k>} = h_j^k \left(\frac{\partial^k f}{\partial x^k}\right)_j,$$

α and β are free parameters. Introducing the vectors

$$F = \{f^{<1>}, f^{<2>}, \ldots, f^{<n>}\}^T, \quad E = \{1, 0, \ldots, 0\}^T,$$

and the matrices

$$A = \frac{1}{2}\begin{pmatrix} \frac{\alpha+\beta\sigma}{1!} & \frac{\alpha-\beta\sigma^2}{2!} & \ldots & \frac{1+(-1)^{n+1}\beta\sigma^n}{n!} \\ 0 & \frac{1-\sigma}{1!} & \ldots & \frac{1+(-1)^{n-1}\sigma^{n-1}}{(n-1)!} \\ 0 & 0 & \ldots & \frac{1+(-1)^{n-2}\sigma^{n-2}}{(n-2)!} \\ \ldots & \ldots & \ldots & \ldots \\ 0 & 0 & \ldots & \frac{1-\sigma}{1!} \end{pmatrix},$$

$$L = \begin{pmatrix} 0 & 0 & 0 & 0 & \ldots & 0 \\ \sigma & 0 & 0 & 0 & \ldots & 0 \\ 0 & \sigma^2 & 0 & 0 & \ldots & 0 \\ 0 & 0 & \sigma^3 & 0 & \ldots & 0 \\ \ldots & \ldots & \ldots & \ldots & \ldots & \ldots \\ 0 & 0 & 0 & \ldots & \sigma^{n-1} & 0 \end{pmatrix}.$$

equations (17) and (18) can be rewritten into a vector form and the following relation can be obtained:

$$-\frac{1}{2}L(\frac{1}{\sigma_j})F_{j-1} + (A+L)F_j - \frac{1}{2}L(\sigma_{j+1})F_{j+1} = \frac{1}{2}(\alpha\delta_x^+ + \beta\delta_x^-)f_j E, \tag{19}$$

L and A are N × N matrices, F and E are N dimensional vectors and $f_j^{<k>}/h_j^k$ approximates $\frac{\partial^k f}{\partial x^k}$ with the accuracy of order $N-k+1$. In the case $\sigma_j = 1$, the coefficients in (19) do not depend on the coordinate direction and the mesh grid points.

By choosing $\alpha = \beta = 1$ and $\sigma_j = 1$ and $\alpha = -\beta = 1$ and $\sigma_j = 1$, the SCFDM relations for odd and even derivatives can be obtained in a uniform grid respectively. For these relations, the plots of modified wave numbers for the first and second derivatives approximation of the SCFDM using Fourier analysis are given in Figures 1 and 2.

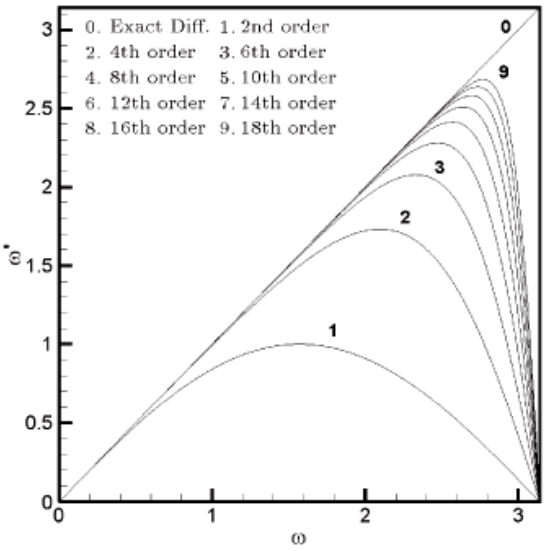

Figure 1. Variations of modified wave number for the first derivative approximation for SCFDM with $\sigma_i = 1$.

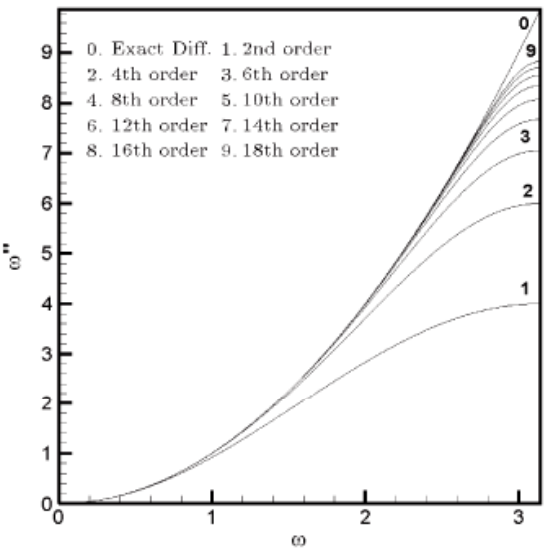

Figure 2. Variations of modified wave number for the second derivative approximation for SCFDM with $\sigma_i = 1$

Numerical Solution

A sixth-order SCFDM formulation for nonuniform grid points has been used to compute the basic flow and the PSE equations. Sixth-order SCFDM formulation for each variable has four relations, one of them is the basic equation and the others are auxiliary equations. In these sets of equations, there are five unknowns $\{f, f', f'', f''', f''''\}^T$ where $(')$ denotes the derivative. The governing equation is needed to close the system and a block tridiagonal system is obtained with a block size 5×5.

Basic Flow Computation

By linearizing the basic flow equation (4) and SCFDM relations and using the Newton method, a block tridiagonal system is obtained which can be solved by the Thomas algorithm. The convergence is quick, and is less than 10 iterations for tolerance of 10^{-12}.

PSE Computation

Numerical solution to PSE equations needs to discretize equations (6) and (14) in both streamwise (x) and wall normal (y) directions. In the streamwise direction, the first-order backward difference scheme is used. In the wall normal direction, the sixth-order SCFDM is employed. For linear PSE, the system of differential equations (6) can be rewritten as below by using the first-order backward difference scheme in streamwise direction:

$$\left(L(\alpha_n) + \frac{1}{\Delta x} M(\alpha_n)\right)[\hat{q}_n] = \frac{1}{\Delta x} M(\alpha_n)[\hat{q}_{n-1}], \quad (20)$$

in which Δx is the stepsize in the x-direction. In equation (20) there are four unknowns and by using a sixth-order SCFDM formulation in y-direction for each unknown, twenty equations are obtained (sixteen SCFDM relations and four governing equations).

These equations require twenty boundary conditions. Equations (11) and (12) provide six boundary conditions. An additional boundary condition is obtained using the derivative of continuity equation at the wall. Other boundary conditions are obtained by using forward and backward SCFDM relations at boundaries. The above system of equations along with the twenty boundary conditions give a block tridiagonal system of equations with a block size of 20×20.

For nonlinear PSE, the above equations can be used for each mode (n, k).

Initial Conditions

The initial conditions for the present computation are obtained by solving the Orr-Sommerfeld equations at the corresponding Reynolds number $R_\circ$ and nondimensional frequency F $(\omega\nu/U_\infty^2 \times 10^6)$. The Orr-Sommerfeld equations in primitive forms can be obtained from the linear PSE equations by setting $\frac{\partial}{\partial x}$

derivatives and V_b equal to zero and can also be solved using super compact method.

The Orr-Sommerfeld eigenfunctions are normalized such that:

$$u'_{\max} = \left(2\hat{u}\hat{u}^{\dagger}\right)^{1/2} = A^{\circ}, \tag{21}$$

and

$$\mathrm{Phs} = \tan^{-1}\left\{\frac{\mathcal{I}(\hat{u})}{\mathcal{R}(\hat{u})}\right\}_{\max} = (\mathrm{Phs})^{\circ}, \tag{22}$$

where A° and $(\mathrm{Phs})^{\circ}$ are initial amplitude and phase which are input parameters to the code.

RESULTS AND DISCUSSION

Here, both linear and nonlinear computations are presented for two cases. All calculations were initiated at $R_{\circ} = 400$, where the shape function and corresponding wave number for the TS wave are provided by the Orr-Sommerfeld (linear quasi-parallel) solutions. All the present computations are performed on PC.

2-D Linear and Nonlinear PSE

The first test case is the evolution of a two-dimensional TS fundamental wave of frequency F = 86 using the linear and nonlinear PSE. The initial amplitude level of the fundamental mode (1F) is chosen to be $A^0_{1,0} = 0.25\%$ based on $u'_{\max}$. For nonlinear calculations, three Fourier components ($N = 2, K = 0$) with frequencies 0F, 1F, 2F are used. The stepsize employed in the downstream marching procedure is $\Delta x = 10$ for both the linear and nonlinear PSE. The results are obtained in the interval $Re = 400$ to $Re = 1000$. Figure 3 shows the amplitude curves based on $u'_{\max}$ versus Reynolds number $Re = U_{\infty}\delta(x)/\nu = \sqrt{U_{\infty}x/\nu} = \sqrt{Re_x}$ for the fundamental mode (1F) and its first harmonic (2F). The upper curve is the amplitude of the TS wave and the lower one is the amplitude of the 2F harmonic. This figure also shows the TS amplitude curve using linear PSE which compares very well with the Bertolotti results [3]. The present results for nonlinear PSE computations are in good agreement with those of Bertolotti [3] and DNS computed by Bertolotti et al. [5]. The differences between the present solutions and those of the Bertolotti results [3] are due to different approximations used in PSE formulation. Bertolotti used stream function formulation and solved the resulting equation using the spectral method. Here, the primitive form is used and is numerically solved by the super compact method. For the nonlinear PSE, the velocity profiles of u' for the MFD wave (0F), the TS wave (1F) and the first harmonic wave are shown in Figure 4 at $Re = 796$. These profiles agree very well with the DNS results by Bertolotti et al. [5]. The present computations for nonlinear PSE are also in good agreement with those of DNS computed by Joslin et al. [13], but for clarity these comparisons are not shown in the figures.

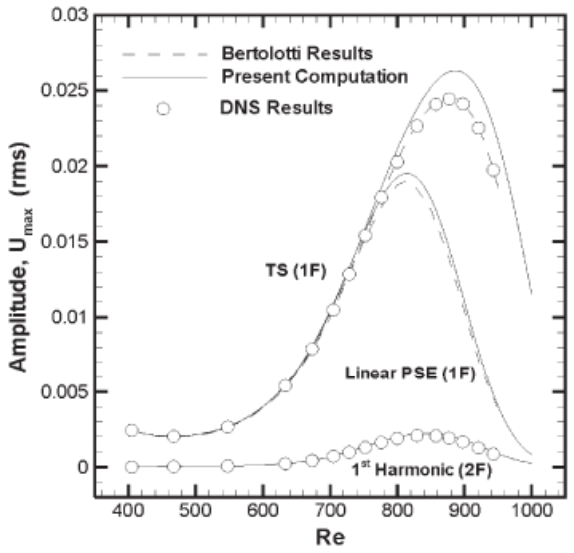

Figure 3. Comparison of amplitudes based on $u'_{\max}$ versus Reynolds number for the TS wave F = 86 using the linear and nonlinear PSE.

3-D Nonlinear PSE

There are different routes to transition depending on the initial conditions. The PSE code developed here can be used all the way to transition for both fundamental (K-type) and subharmonic (H-type) breakdown. The most dangerous route is expected to be a three-dimensional subharmonic mode interaction. To demonstrate the ability of the PSE in predicting the onset of transition, a nonlinear interaction is considered between a TS fundamental wave (mode (2,0)) 2F = 124, and a pair of subharmonic oblique waves ((1,1) and (1,-1) modes) for conditions of Kachanov and Levchenko experiment [14]. The initial amplitudes of

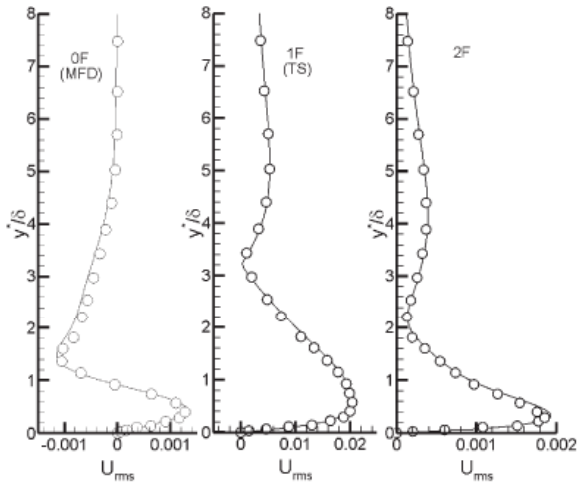

Figure 4. Comparison of velocity profiles of u' for various modes at $Re = 796$ and F = 86. Circles denote results from DNS simulation by Bertolotti et al. [5].

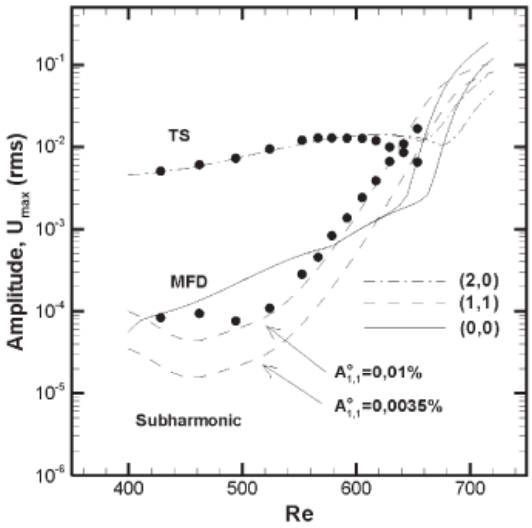

Figure 5. Comparison of amplitudes based on $u'_{\max}$ versus Reynolds number for subharmonic breakdown (2F = 124 and $\beta = 0.14$). Dots denote experimental data.

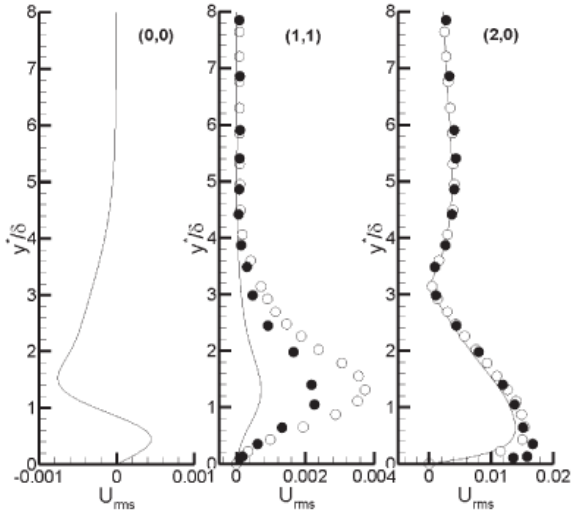

Figure 6. Comparison of velocity profiles of u' for various modes at $Re = 608$ and 2F = 124. Circles denote DNS results by Fasel et al. [15] and dots are experimental data.

the TS wave and the subharmonic wave are chosen $A^{\circ}_{2,0} = 0.46\%$ and $A^{\circ}_{1,1} = 0.0035\%$ based on $u'_{\max}$, respectively. The spanwise wave number of the subharmonic mode is fixed at $\beta = 0.14$. The stepsize for the marching procedure is $\Delta x = 15$. The solution is obtained with Fourier series truncated to $N = 2$, and $K = 1$, and extended from $Re = 400$ to $Re = 720$. To investigate the effect of initial amplitude of subharmonic mode on the solution, the results are also presented for $A^{\circ}_{1,1} = 0.01\%$. For subharmonic breakdown, based on initial amplitudes of subharmonic mode we have $A^{0}_{1,1} = 0.0035\%, 0.01\%$. Figure 5 shows the PSE results for the amplitudes of three modes (0,0), (1,1) and (2,0) based on $u'_{\max}$ together with experimental data for H-type breakdown. Amplitudes were measured at $\eta = 1.3$. The agreement is remarkable for the TS wave (2,0). The amplitude curve for the subharmonic mode with initial amplitude $A^{0}_{1,1} = 0.01\%$ is in better agreement than $A^{0}_{1,1} = 0.0035\%$. The results demonstrate that the solution depends on the initial amplitude of subharmonic mode only in the transition region ($Re > 630$) where the MFD mode rapidly rises thereafter. The velocity profiles of u' for three modes at Re=608 for $A^{0}_{1,1} = 0.01\%$ are shown in Figure 6. Good agreement in the amplitude profiles are found between the present results and the DNS computed by Fasel et al. [15] and also the experimental data especially for the TS wave. The differences between the PSE and the experimental results for subharmonic mode may result from the initial conditions which are provided by the Orr-Sommerfeld equations. Although not shown here, the present solutions have been compared with those of DNS computed by Joslin et al. [13] and have shown good agreement. Figure 7 presents the variations of nondimensional displacement thickness versus Reynolds number for the subharmonic breakdown. This figure shows the results of unperturbed and perturbed flows. As shown in this figure, near the onset of transition, the displacement thickness originally increases very little and then decreases. Figure 8 presents the variations of nondimensional skin friction coefficient versus Reynolds number for the subharmonic breakdown. The skin friction coefficient calculated by the nonlinear PSE has a minimum at $Re = 670$ for $A^{\circ}_{1,1} = 0.0035\%$ and is shifted back to $Re = 650$ for $A^{\circ}_{1,1} = 0.01\%$. The figure also shows comparison of the results with those obtained by fourth-order compact method [17], which indicates the accuracy of the present computation. The rise of

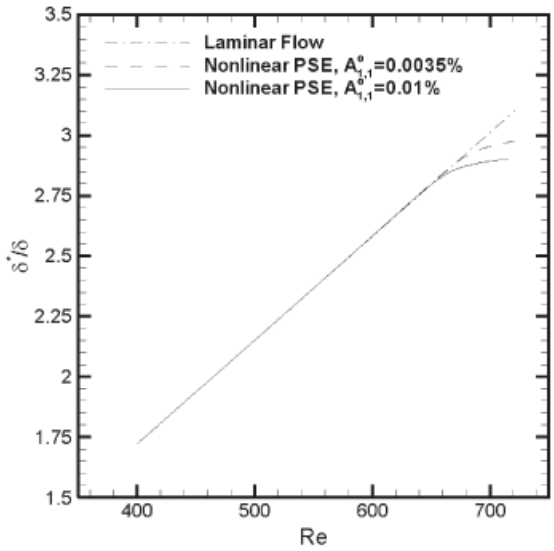

Figure 7. Variation of nondimensional displacement thickness versus Reynolds number for subharmonic breakdown.

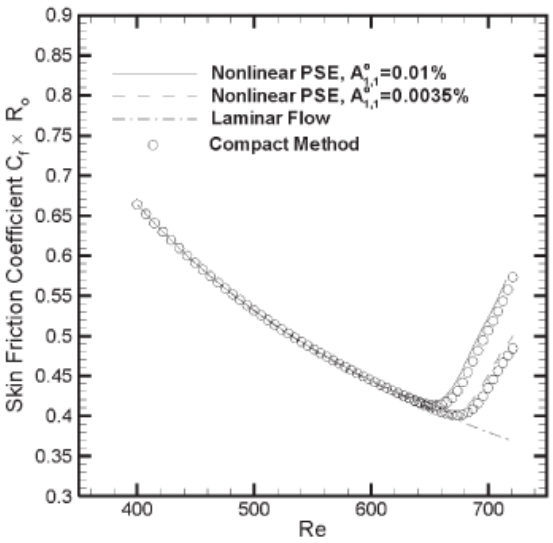

Figure 8. Comparison of nondimensional skin friction coefficient versus Reynolds number for subharmonic breakdown. Circles denote 4^{th}-order Compact method results by Esfahanian et al. [17].

skin friction due to the MFD indicates the onset of transition in the sense of operational definition.

Calculation of the CPU time for different simulations of the linear and nonlinear PSE equations using super compact scheme shows that the developed code is computationally very efficient. For example the computational cost of the 3-D nonlinear PSE (with 200 grid points), which is the most difficult case, takes only 74 seconds on an ordinary personal computer (P4, 3Ghz). Furthermore, the comparison of computational cost of the sixth-order super compact and fourth-order compact [17] methods, shows that the super compact is 3 times more expensive than the fourth-order compact scheme.

CONCLUSIONS

The stability analysis of the Blasius boundary layers on a flat plate has been studied using linear and nonlinear PSE. Both linear and nonlinear PSE equations have been solved using super compact method and primitive variables. The agreement of the present results with the previous works, the direct numerical solutions, and the experiment is very good. The linear and the nonlinear results show that the PSE approach is a powerful tool for the study of boundary layer stability and prediction of transition location.

ACKNOWLEDGMENT

The authors would like to thank University of Tehran for the financial support of this research.

REFERENCES

1. Herbert, Th., "Boundary-Layer Transition - Analysis and Prediction Revisited", *AIAA Paper 91-0737*, (1991).
2. Herbert, Th., "Parabolized Stability Equations", *Annu. Rev. Fluid. Mech.*, **29**, PP 245-283(1997).
3. Bertolotti, F. P., "Linear and Nonlinear Stability of the Boundary Layers with Streamwise Varying Properties", Ph.D. Thesis, The Ohio State University, Columbus, Ohio(1991).
4. Chang, C. -L., Malik, M. R., Erlebacher, G. and Hussaini, M. Y., "Compressible Stability of Growing Boundary Layers Using Parabolized Stability Equations", *AIAA Paper 91-1636*, (1991).
5. Bertolotti, F. P., Herbert, TH., Spalart, P. R., "Linear and Nonlinear Stability of the Blasius Boundary Layer", *J. Fluid Mech.*, **242**, PP 441-474(1992).
6. Herbert, Th., and Bertolotti, F. P., "Stability Analysis of Nonparallel Boundary Layers", *Bull. Amer. Phys. Soc.*, **32**, PP 2079(1987).
7. Dexun, Fu, Yanwen, Ma, "High Resolution Schemes", *Computational Fluid Dynamic Review*, M. Hafez and K. Oshima, John Wiley & Sons, Inc., (1995).
8. Yanwen, Ma and Dexun, Fu, "Super Compact Finite Difference Method (SCFDM) with Arbitrary High Accuracy", *Computational Fluid Dyn. J.*, **5(2)**, PP 259-276(1996).
9. Dexun, Fu and Yanwen, Ma, "Analysis of Super Compact Finite Difference Method and Application for Simulation of Vortex-Shock Interaction", *Int. J. for Numerical Methods In Fluids*, **36**, PP 773-805(2001).
10. Ghader, S., "Numerical Simulation of the Stability of the Laminar Boundary Layer Flow Over a Flat Plate by PSE Equations Using Super Compact Method", M.Sc. Thesis, University of Tehran(2000).
11. Esfahanian V., Ghader S. and Kh. Ashrafi, "Accuracy Analysis of Super Compact Scheme in Nonuniform Grid with Application to Parabolized Stability Equations", *Int. J. Numer. Meth. Fluids*, **46**, PP 485-505(2004).
12. Esfahanian V., Ghader S., and Mohebalhojeh A. R., "On the Use of Super Compact Scheme for Spatial Differencing in Numerical Models of the Atmosphere", *Q. J. Roy. Meteorl. Soc.*, **131**, PP 2109-2130(2005).
13. Joslin, R. D., Chang, C. L., and Streett. C. L., "Spatial Direct Numerical Simulation of Boundary-Layer Transition Mechanisms: Validation of PSE Theory", *Theoret. Comput. Fluid Dynamics*, **3**, PP 271-288(1993).
14. Kachanov, Y. S., and Levchenko, V. Y., "The Resonant Interaction of Disturbances at Laminar-Turbulent Transition in a Boundary Layer", *J. Fluid Mech.*, **138**, (1984).
15. Fasel, H. F., Rist, U., and Konzelmann, U., "Numerical Investigation of the Three-Dimensional Development in Boundary-Layer Transition", *AIAA J.*, **28(1)**, PP 29-37(1990).

16. Malik, M. R., Chuang, S., and Hussaini, M. Y., "Accurate Numerical Solution of Compressible, Linear Stability Equations", *ZAMP*, **33**, PP 189(1982).

17. Esfahanian V., Hejranfar K. and Sabetghadam F., "Linear and Nonlinear PSE for Stability Analysis of the Blasius Boundary Layer Using Compact Scheme", *ASME J. Fluids Eng.*, **123(3)**, PP 545-550(2001).

18. White, F., M., *Viscous Fluid Flow*, MC Graw-Hill, (1991).